Analysis of Birefringence Decay Profiles for Nucleic Acid Helices Possessing Bends: The τ-Ratio Approach

Elsi Vacano and Paul J. Hagerman
Department of Biochemistry and Molecular Genetics, University of Colorado Health Sciences Center, Denver, Colorado 80262 USA

ABSTRACT For nucleic acid helices in the 100–200-bp range, a central bend or point of flexibility increases the rate of rotational diffusion. In a transient electric birefringence (TEB) experiment, this increase is manifest as a reduction in the terminal (slowest) birefringence decay time. Previous experimental and theoretical work has demonstrated that the ratio of the decay times for a bent/flexible molecule and its fully duplex (linear) counterpart represents a sensitive, quantifiable measure of the apparent bend angle (τ-ratio approach). In the current work, we have examined the influence of helix parameters (e.g., persistence length, helix rise, diameter) on the τ-ratio for a given bend. The τ-ratio is found to be remarkably insensitive to variations and/or uncertainties in the helix parameters, provided that one employs bent and control molecules with the same sequence and length (apart from the bend itself). Although a single τ-ratio determination normally does not enable one to distinguish between fixed and flexible bends, such a distinction can be made from a set of τ-ratios for molecules possessing two variably phased bends. A number of additional uncertainties are examined, including errors in the estimation of the dimensions of nonhelix elements that are responsible for bends; such errors can, in principle, be estimated by performing a series of measurements for molecules of varying length.

INTRODUCTION

Transient electric birefringence (TEB) is a sensitive method for characterizing the global conformations and flexibility of DNA and RNA molecules in solution (reviews: Fredericq and Houssier, 1973; O'Konski, 1976; Charney, 1988; Hagerman, 1996). In a typical TEB experiment, one measures the rate of decay of solution birefringence after the removal of an orienting electric field pulse; the decay of the signal reflects the randomization of the nucleic acids through (Brownian) rotational diffusion. To underscore the sensitivity of the TEB method, Mellado et al. (1988) have pointed out that for rods possessing a central, flexible hinge, the fractional change in the longest rotational relaxation time (relative to the rigid, unbent rod) is more than an order of magnitude greater than the corresponding change in the translational diffusion coefficient. Over the past decade, TEB (and the related electrooptic method, transient electric dichroism, TED) has been used to characterize particular sequence elements in DNA (Diekmann et al., 1982; Hagerman, 1984; Levene et al., 1986; Stellwagen, 1991; Porschke et al., 1993).

More recently, TEB has been used to quantify interhelix angles in branched DNA (Cooper and Hagerman, 1989) and in RNA (e.g., Friederich et al., 1995; Amiri and Hagerman, 1994; Leehey et al., 1995; Zacharias and Hagerman, 1995a,b, 1996; review: Hagerman, 1996). Most of these

latter investigations have exploited the fact that a molecule possessing a bend experiences more rapid rotational diffusion than does a linear molecule with the same contour length and sequence apart from the bend. In a typical experiment, two DNA or RNA molecules are constructed that differ only by the presence of a nonhelix element at the center of one of the molecules (heteroduplex construct; htx) (Fig. 1 A) and an equivalent length of helix at the center of the second molecule (reference duplex; dplx). The two molecules are otherwise identical in length and sequence. Birefringence decay profiles are determined for both molecules (Fig. 1 B), from which the ratio of their terminal decay times, τ_{htx}/τ_{dplx}, is obtained as the principal experimental observable. Finally, these experimentally derived ratios are compared with curves of computed τ-ratios, determined as a function of the central bend angle for wormlike chains having the same intrinsic properties (e.g., axial ratio, flexibility, etc.) as the helix (Fig. 1 C).

Much of the early motivation for the development of hydrodynamic theory for broken rods has derived from experimental studies of proteins possessing segmental flexibility (e.g., myosin) (Highsmith et al., 1977, 1982; Garcia de la Torre and Bloomfield, 1980; Harvey and Cheung, 1982). There has been extensive theoretical development of the hydrodynamics of flexible and rigidly bent rods, with more recent treatments combining the fixed and elastic character of the central bend with full hydrodynamic interactions between and within subunits (Harvey and Cheung, 1980; Wegener et al., 1980; Wegener, 1982a,b; Mellado and Garcia de la Torre, 1982; Harvey et al., 1983; Garcia de la Torre et al., 1985; Wegener, 1986; Mellado et al., 1988; Iniesta et al., 1988; Garcia Molina et al., 1990).

Although close parallels between the current and previous work will be noted in subsequent sections, several
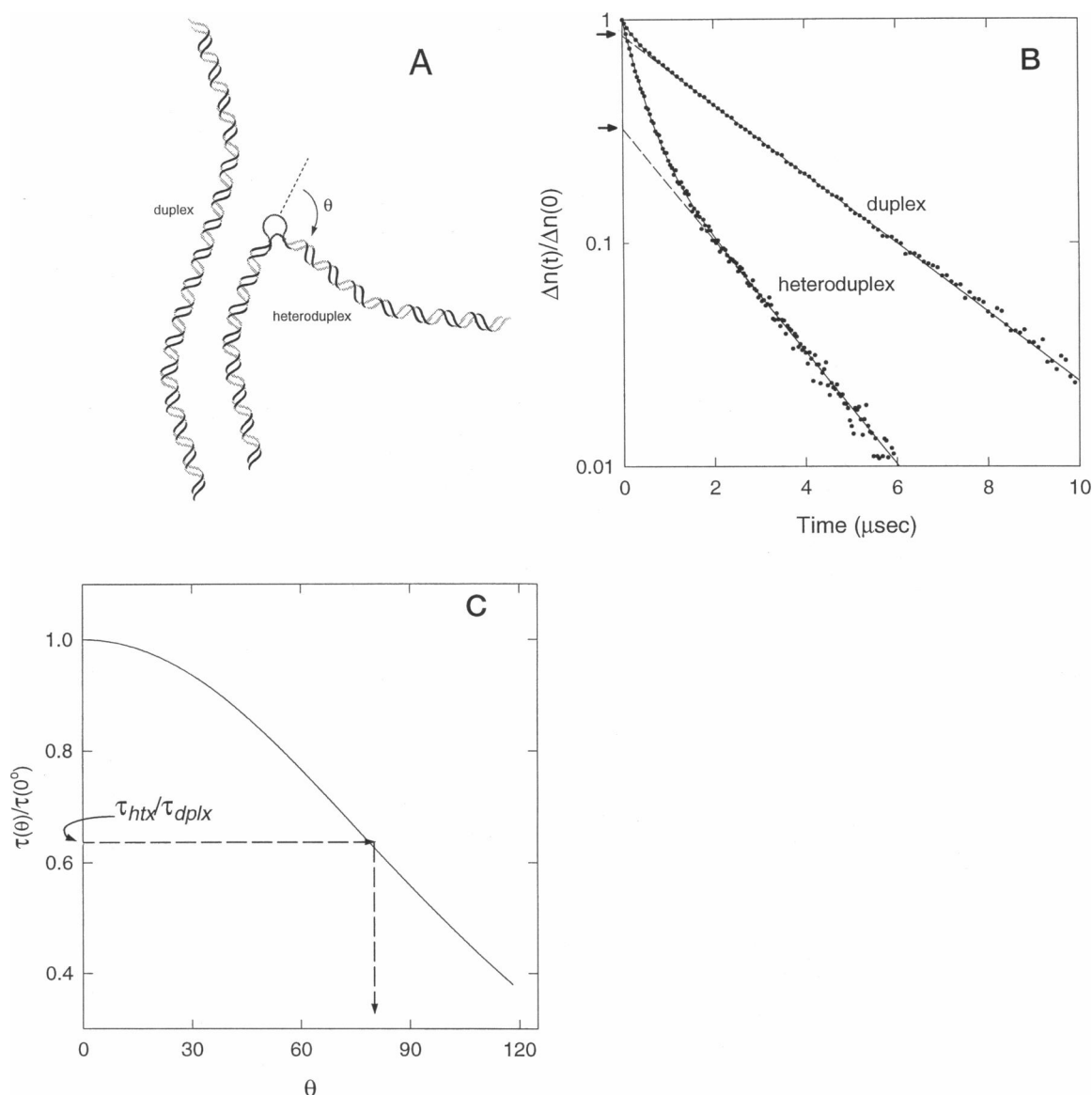
FIGURE 1   Principal features of the τ-ratio method. (A) Two nucleic acid helices are compared that are identical, except for the presence of a nonhelix or altered-helix element at the center of one molecule (heteroduplex, htx) and an equivalent length of helix at the center of the second (duplex, dplx) molecule. The nonhelix element gives rise to a bend, θ, which may also reflect increased local flexibility. (B) Representative (normalized) birefringence decay profiles for a 148-bp duplex RNA molecule, either with or without a central U_6 bulge (*lower and upper curves*, respectively) (adapted from figure 2 of Zacharias and Hagerman, 1995a). Information regarding the degree of bending and/or flexibility of the central nonhelix element derives in part from the ratio of the terminal (slow) decay times of the heteroduplex and duplex species [τ_{htx}/τ_{dplx}]. Solid lines indicate two-exponential fits to the experimental decay profile. Extensions of terminal components are indicated by dashed lines and arrows. (C) The relationship between the observed τ-ratio and bend angle, θ, is provided through computational models whereby τ-ratios are determined as a function of θ (see text, Methods).

observations from the earlier studies provide general support for the τ-ratio approach:

1. Mellado et al. (1988) demonstrated that for macromolecules possessing a central hinge, neglect of hydrodynamic interactions between the two segments results in less than a 10% difference in the slowest rotational decay time. Thus the τ-ratio should be quite insensitive to the specific form of the hydrodynamic interaction employed in the τ-ratio analysis, except perhaps for the most acute intersegment angles.

2. Garcia Molina et al. (1990) demonstrated that even though the absolute value for the slowest rotational diffu-

sion time depends to a significant extent on the number of beads (N) employed in the model, varying by 30% between 10 and 50 beads for rigid to moderately flexible chains, there was virtually no change in the ratio between rigid and flexible chains over the same range of N. This invariance of the ratio with bead number provides strong theoretical support for approaches involving ratios between linear and bent molecules, even when the intrinsic properties of the chain itself are imperfectly defined.

3. Garcia Molina et al. (1990) argued that the ratio of the decay times for the rigid versus flexible chains would re-

main essentially unchanged in passing from a bead to a cylindrical profile, again arguing that the τ-ratio is a specific characteristic of the central bend.

4. Finally, the computed τ-ratio for rods with fixed bends decreased by roughly fivefold as the bend angle increased from 0° to 180° (Wegener, 1986; Iniesta et al., 1988), underscoring the sensitivity of the τ-ratio to the magnitude of the central bend.

To strengthen the theoretical underpinnings of the τ-ratio approach, the current analysis will extend two aspects of the previous hydrodynamic models. First, prior treatments of the broken rod have regarded the individual rod segments as rigid; however, for nucleic acid helices flanking a bend or hinge, the individual helix segments possess significant flexibility (reviews: Hagerman, 1988, 1997). The influence of various helix parameters on the τ-ratio will therefore be examined. Second, the principal experimental outcome of a single set of TEB measurements (the τ-ratio) is unlikely, in general, to provide a clear distinction between fixed and flexible central bends. Accordingly, the influence of various combinations of static and dispersive character of the bend will be examined from the perspective of their influence on the τ-ratio, and additional methods designed to distinguish between static and dispersive character will be proposed.

The current analysis is based on an "equilibrium-ensemble" approach (Hagerman and Zimm, 1981) in which the principal diffusion coefficients are generated for each instantaneous, rigid-body configuration for individual chains within the ensemble. The conformations of chains in the ensemble are determined by the intrinsic properties of the chain and by additional bends. The birefringence decay times are subsequently determined from the ensemble averages of the principal diffusion coefficients (see Methods). The validity of the equilibrium-ensemble approach had been considered previously (Kramers, 1946; Zimm, 1980) and has received quantitative support from theoretical studies of diffusion dynamics (Roitman and Zimm, 1984a,b; Roitman, 1984; Allison and Nambi, 1992). As a fundamentally static representation of the diffusion process, the equilibrium-ensemble approach does not address the issue of the internal dynamics of the polymer chains, except to assume that such interconversions are rapid compared to the overall decay process. This assumption receives experimental support from the close agreement in values of the persistence length (DNA) obtained from TEB (TED) and ligase-catalyzed cyclization measurements (e.g., Levene et al., 1986; Taylor and Hagerman, 1990), the latter representing a nonhydrodynamic approach. Porschke et al. (1993) have suggested, however, that such interconversions may be slow for certain sequences (see also, Shen and Hagerman, 1994)—an issue that must be addressed through additional experimental work.

This study makes no assumptions regarding the orienting mechanism, because the birefringence decay times (but not the amplitudes) are assumed to be independent of the nature of the orienting forces for sufficiently low fields (e.g., Wegener et al., 1979; Wegener, 1986); the issue of ampli-

tudes is considered further in the following article (Zacharias and Hagerman, 1997). In fact, the experimental observation that the decay times and amplitudes for bent/branched RNA molecules are generally independent of the strength of the orienting field (for low to moderate fields) (Hagerman, 1996, and references therein) argues that the experimental decay times reflect the unperturbed (equilibrium) distribution of chain contours.

Finally, it should be noted that whereas reference helix parameters for RNA are used for most of the examples presented herein, the results of the current work apply equally to DNA, as is made explicit in several of the figures. In fact, the results are exceedingly insensitive to the choice of helix parameters—a principal advantage of the τ-ratio approach—provided that the same parameters apply to both duplex (control) and heteroduplex molecules.

METHODS

Generation of individual chain contours

The coordinate representations for individual base pairs, as well as the coordinate transformations between adjacent base pairs, are exactly as defined in Hagerman and Ramadevi (1990). In particular, tilt (ω_i), roll (θ_i), and twist (φ_i) represent right-handed rotations about the local x_i, y_i, and z_i axes, respectively. The local coordinate frame of the ith base pair is transformed into the ($i - 1$)st frame by application of the transformation matrix, A_i, which comprises successive tilt, roll, and twist operations; specifically, $A_i = a_i(\varphi)a_i(\theta)a_i(\omega)$. Each of the elementary rotations is composed of static and stochastic components. Thus a roll deformation between the ith and ($i - 1$)st base pair is given by $\theta_i = \theta_{i,o} + \delta\theta_i$, where $\theta_{i,o}$ is the static (fixed) component, and where $\langle(\delta\theta_i)^2\rangle$ is the variance of normally distributed fluctuations about $\theta_{i,o}$. The variances, $\langle(\delta\theta_i)^2\rangle$ and $\langle(\delta\omega_i)^2\rangle$ are specified by the relation $\langle(\delta\theta_i)^2\rangle + \langle(\delta\omega_i)^2\rangle = 2h/P$, where h is the helix rise and P is the persistence length. Implicit in this expression is the absence of a preferred direction of angular dispersion. Although an oversimplification, this assumption is not expected to significantly affect the conclusions of the current work. Note that as defined herein, P describes elastic deformations about a static chain contour; thus P is not influenced by static bends. The twist variance, $\langle(\delta\varphi_i)^2\rangle$, is defined by the relationship $\langle(\delta\varphi_i)^2\rangle = kTh/C$, where k is Boltzmann's constant, T is the temperature (= 298°K), and C is the torsional elastic constant. Lateral and torsional flexibilities are thus introduced through P and C, respectively. Whenever a central region of increased flexibility is introduced, the persistence length within that region is referred to as P_{ctr}, with the standard (reference) persistence length of the remaining helix explicitly referred to as P_{ref}.

Hydrodynamic model

The hydrodynamic model employed in the current work is essentially identical to the model utilized by Hagerman and

Zimm (1981). Because the underlying hydrodynamic theory is outlined by Hagerman and Zimm (1981) and is more fully discussed in an excellent review by Garcia de la Torre and Bloomfield (1981), it will not be repeated here; however, several aspects of the computational model will be summarized in the following paragraphs.

The helix is represented by a string of virtually touching Stokes' spheres (beads) that are arranged along the chain contour. The sphere radius is adjusted to yield an average volume (per unit length) that is equal to the volume of a cylinder with a specified hydrodynamic radius. The "virtual" designation refers to the fact that for chain lengths that do not accommodate an integral number of spheres, the remaining spheres are equally spaced along the chain contour. Unless specified otherwise, the cylinder radius (representing the radius of the hydrated helix) is set to 13 Å. Intrachain hydrodynamic interactions among the beads are computed using the Rotne-Prager hydrodynamic interaction tensor for nonoverlapping beads of equal radii (Rotne and Prager, 1969; Garcia de la Torre and Bloomfield, 1981) (the following expression corrects typographical errors present in the expression for T_{ij} given by Hagerman and Zimm (1981)):

$$\tilde{T}_{ij} = (8\pi\eta_o r_{ij})^{-1}\left[\left(\tilde{I} + \frac{\vec{r}_{ij}:\vec{r}_{ij}}{r_{ij}^2}\right) + \frac{2\sigma^2}{r_{ij}^2}\left(\frac{1}{3}\tilde{I} - \frac{\vec{r}_{ij}:\vec{r}_{ij}}{r_{ij}^2}\right)\right] \quad (1)$$

where $\vec{r}_{ij}$ and r_{ij} are the vectorial and scalar separations between spheres i and j, $\vec{r}_{ij}:\vec{r}_{ij}$ is the dyadic product of the corresponding interbead vector, $\tilde{I}$ is the unit (3 × 3) tensor, σ is the sphere radius, and η_o is the macroscopic solvent viscosity. $\tilde{T}_{ij}$ scales the velocity perturbation (i.e., hydrodynamic coupling) at the location of sphere i due to forces on bead j (e.g., Hagerman and Zimm, 1981; Garcia de la Torre and Bloomfield, 1981).

As noted above, the current model neglects the hydrodynamic consequences of bead overlap at the bend center. This approximation is not expected to have a significant effect on the τ-ratios, because the bend center(s) generally lie near the center of hydrodynamic resistance. This expectation is supported by the absence of any length-dependent effect on the τ-ratios for molecules with acute bends (see Fig. 3). Finally, bead overlap between distal regions of an individual chain (excluded volume effects) is treated by excluding such chains from the ensemble. This situation arises for flexible chains that possess substantial bends; such effects become significant mainly for bends that are greater than 90° and for L/P ratios greater than 1.0.

The friction tensor, ζ, for pure rotation is computed for each chain in an ensemble, as described previously (Hagerman and Zimm, 1981). Diagonalization of ζ yields the three principal diffusion coefficients through the Einstein relations, $D_i = kT/\zeta_i$ ($i = 1-3$). The ensemble-average, terminal decay time is obtained from the relation, $1/\tau = 3(\langle D_1 \rangle + \langle D_2 \rangle)$, where $\langle D_1 \rangle$ and $\langle D_2 \rangle$ are the two smallest diffusion coefficients, averaged over all chains in the ensemble. The quantitative validity of the above expression

for τ has been discussed elsewhere (Hagerman and Zimm, 1981; Roitman and Zimm, 1984b; Zacharias and Hagerman, 1997) and is expected to be accurate to within ~5% for single τ estimations. For τ-ratio estimates, the errors should be partially self-cancelling and therefore smaller.

Computational methods

Ensembles of chains for each set of helix parameters comprise 2000–5000 individual chains. Generation of ensembles is initiated by specifying the following parameters (default/reference values in parentheses): P (700 Å), C (3.0 × 10^{-19} erg-cm), h (2.8 Å; 2.8 × 10^{-8} cm), $\theta_{o,i}$ and $\omega_{o,i}$ (0°, all i), $\varphi_{o,i}$ (30°, all i), and hydrodynamic radius (13 Å). Bends are introduced through nonzero values of $\theta_{o,i}$ for specified positions (default, central base-pair transition). Alterations in flexibility are introduced through variation in P_i for specified base-pair positions. Variations in other helix parameters are as specified in the text and figure legends. Computations were performed on Silicon Graphics 4D25G and Indigo 2 (R10000) workstations.

RESULTS

The ratio of the terminal decay times for bent and linear helices is remarkably insensitive to intrinsic helix parameters

One of the principal advantages of measuring τ-ratios is that the influence of bends on overall polymer conformation can be separated from the intrinsic properties of the surrounding helix (Figs. 2, 3). This separation is of practical importance for two reasons. First, it reduces the impact of errors in the choice of helix parameters such as rise, hydrodynamic radius, and persistence length that are used for the computational models. Thus, whereas an error of 0.2 Å/bp in the assumed value of the helix rise would lead to errors of ~15% for the individual, computed decay times (Fig. 2 A), such an error would have almost no effect on the τ-ratio (Fig. 2 B) or on the derived value for the central bend. Moreover, provided that the helices flanking the central element are long compared to the element itself, errors in the estimated span of the nonhelix element can be kept small (see below) (Friederich et al., 1995; Zacharias and Hagerman, 1996).

Second, the relative constancy of the τ-ratio plots (Fig. 3) enables one to express the results of a large number of computations in terms of relatively simple relations between the observable, τ_{htx}/τ_{dplx}, and the apparent bend angle, θ. Thus, for an experimental τ-ratio [$\tau_{htx}/\tau_{dplx} = R$], a suitable interpolation function for the bend angle (in degrees) is given by

$$\theta = a \times \cos^{-1}(R) + b \times [\sin^{-1}(1 - R)]^c \quad (2)$$

where $a = 1.46$, $b = 0.005$, and where the remaining parameter, c, fluctuates around 2.3, depending on the choice of helix parameters (Table 1). Also depicted in Fig. 3 (*lower*
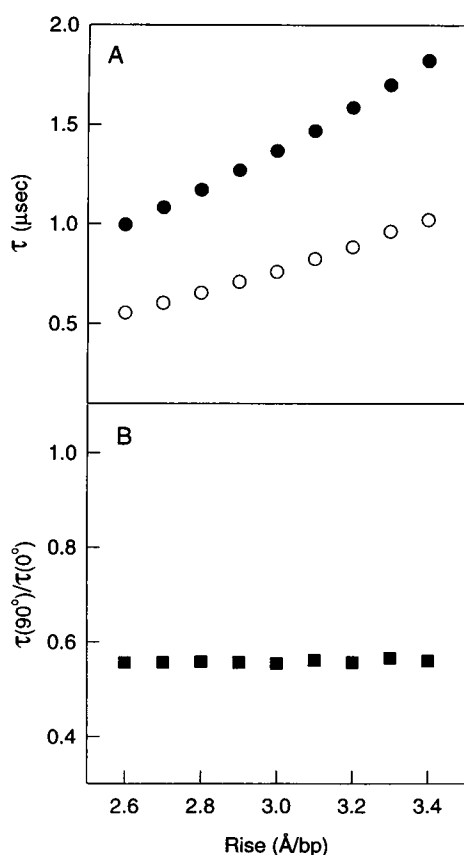
FIGURE 2   (A) Computed terminal decay times for a 140-bp helix (●), and the same molecule with a central, 90° bend (○), plotted as a function of the helix rise. (B) Plot of the ratio, $\tau(90)/\tau(0)$, as a function of helix rise (■). For this set of computations, the hydrodynamic radius is 13 Å, and the persistence length 700 Å.

FIGURE 3   Set of nine plots of the computed τ-ratio as a function of the magnitude of a central, fixed angle, θ_0, for various values of helix length (bp), rise, hydrodynamic radius, and persistence length. In each instance, identical parameters are used for reference and heteroduplex (bent) helices; unless specified, default parameters are rise, 2.8 Å/bp; hydrodynamic radius, 13 Å; persistence length, 700 Å. Plots in the top row indicate variations in rise: ●, 2.6 Å/bp; ■, 3.0 Å/bp; ▲, 3.4 Å/bp. Plots in the second row indicate variations in hydrodynamic radius: ●, 11 Å; ■, 13 Å; ▲, 15 Å. Plots in the bottom row indicate variations in persistence length: ●, 400 Å; ■, 700 Å; ▲, 1000 Å. Included in the central plot are corresponding ratios for helix parameters approximating those of DNA (rise, 3.4 Å; hydrodynamic radius, 13 Å; persistence length, 500 Å) (□). Included in the bottom row plots (variation in flexibility) are corresponding ratios for rigid, bent rods (◇) (Wegener, 1986; Iniesta et al., 1988).

panels) are the results of previous computations for completely rigid, bent rods (Wegener, 1986; Iniesta et al., 1988). These latter data underscore the insensitivity of the τ-ratio to helix parameters. Finally, it should be noted that for larger molecules, and for smaller values of P, there is a slight upward flaring of the computed τ-ratio curves for more acute angles. This effect is due in part to excluded-volume effects between distal portions of the chains.

Additional, isotropic flexibility at the bend locus influences the apparent bend angle derived from single τ-ratio measurements

Interhelix angles created by various nonhelix elements (e.g., bulges) should not be regarded as completely rigid, because such elements will, in general, possess at least as much intrinsic flexibility as that of the surrounding helix. Thus any reported angle will be associated with a certain degree of angle dispersion, at least the equivalent of one or two base pairs on each side of the element under study. This would amount to about $(1.4-2) \times 5.1° \approx 7-10°$ for RNA, where 5.1° represents the rms fluctuation per base pair in an RNA helix of persistence length 700 Å (Kebbekus et al., 1995).

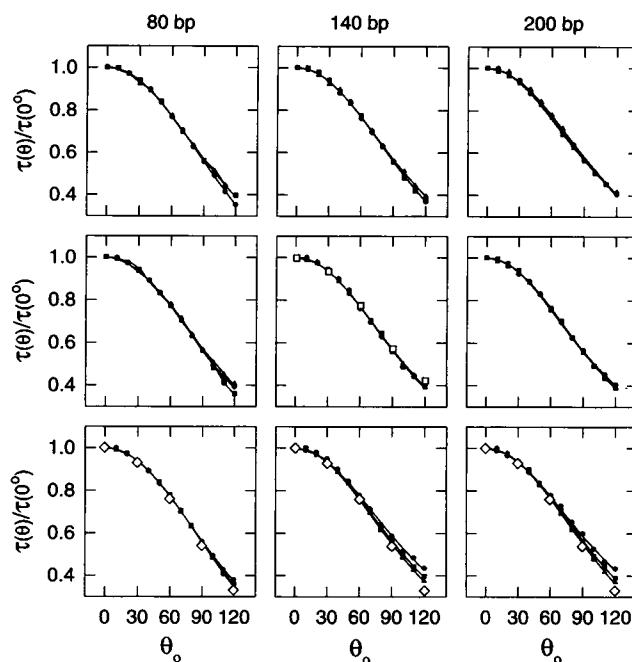For a well-defined angle of minimum energy, any increase in angle dispersion will tend to shift the rms angle toward 90° from either very small or very large angles. This shift reflects the greater sector volumes as the angle approaches 90°, with the attendant gain in configurational entropy (see Schellman, 1974). A second factor, polymer self-exclusion (due to the overlap of the two ends of an individual chain), results in a shift away from very acute angles. This factor is considered in the current hydrodynamic computations (see Methods). A third factor is the nature of the ensemble average. The average is taken over the diffusion coefficients for the individual members of the ensemble, with the contributions of individual chains weighted in proportion to their $1/\tau$ values. As a consequence, the averaging process always introduces a bias toward larger bend angles (more acute interhelix angles, hence smaller τ values).

The greatest shift in apparent angle occurs for the case of zero fixed bend in the presence of added isotropic flexibility (rms angle > 0) (Fig. 4). In this case, both the rms average and the diffusion average over the ensemble will bias the

TABLE 1   Values for the fitting parameter, c, in the empirical relationship* between τ_{htx}/τ_{dplx} and the apparent bend angle for various helix parameters

	c (80 bp)[#]	c (140 bp)	c (200 bp)
Radius (Å)			
11	2.30	2.30	2.32
13	2.23	2.31	2.29
15	2.33	2.32	2.29
Avg = 2.30 ± 0.01			
Rise (Å/bp)			
2.6	2.32	2.25	2.33
3.0	2.23	2.26	2.33
3.4	2.31	2.32	2.36
Avg = 2.30 ± 0.01			
Persistence length (Å)			
400	2.28	2.41	2.40
700	2.24	2.31	2.30
1000	2.22	2.25	2.24

*The relationship between θ (degrees) and R ($=\tau_{htx}/\tau_{dplx}$) is well described by $\theta = 1.462 \cos^{-1}(R) + 0.005[\sin^{-1}(1 - R)]^c$, where c is given in the table for various values of the helix parameters. The default parameters are radius, 13 Å; rise, 2.8 Å/bp; persistence length, 700 Å. Values of c were obtained by curve fitting in SigmaPlot (Jandel Scientific), using the calculated values of $\tau(\theta)/\tau(0°)$ for various sets of parameters and chain lengths. No average for c has been reported for variations in persistence length, because small differences in the curves are evident (Fig. 3) for the longer chains.

[#]Total chain length; bend located at center of chain.

apparent angle toward larger values. This is a very important case to consider separately, because a τ-ratio near 1.0 implies both that the angle is near zero and that the nonhelix element does not possess additional flexibility. As the fixed bend angle increases, the magnitude of the bias decreases (Fig. 5), because the shift in the rms angle approaches zero at a fixed angle of 90°. For fixed angles larger than 90°, the shift in the rms average opposes the shifts due to self-exclusion and diffusion-averaging, leading to a very small total bias, even for a 10-fold reduction in local rigidity (Fig. 5). This issue will be addressed further in the accompanying paper (Zacharias and Hagerman, 1997). This example is necessarily idealized, because angular dispersion for a flexible nonhelix element need not be isotropic, its dimensionality may or may not be restricted, and the rates of equilibration among conformers may vary widely (see Shen and Hagerman, 1994). Nevertheless, the example illustrates the direction of bias, and should serve as a point of departure for additional experimental work.

Apparent bend angles are subject to errors due to uncertainties in the estimated size of the nonhelix element—such errors decrease with increasing helix length

Implicit in the use of the τ-ratio approach is the assumption that the contour lengths of the bend-containing and duplex control molecules are identical. For simple bulge-induced
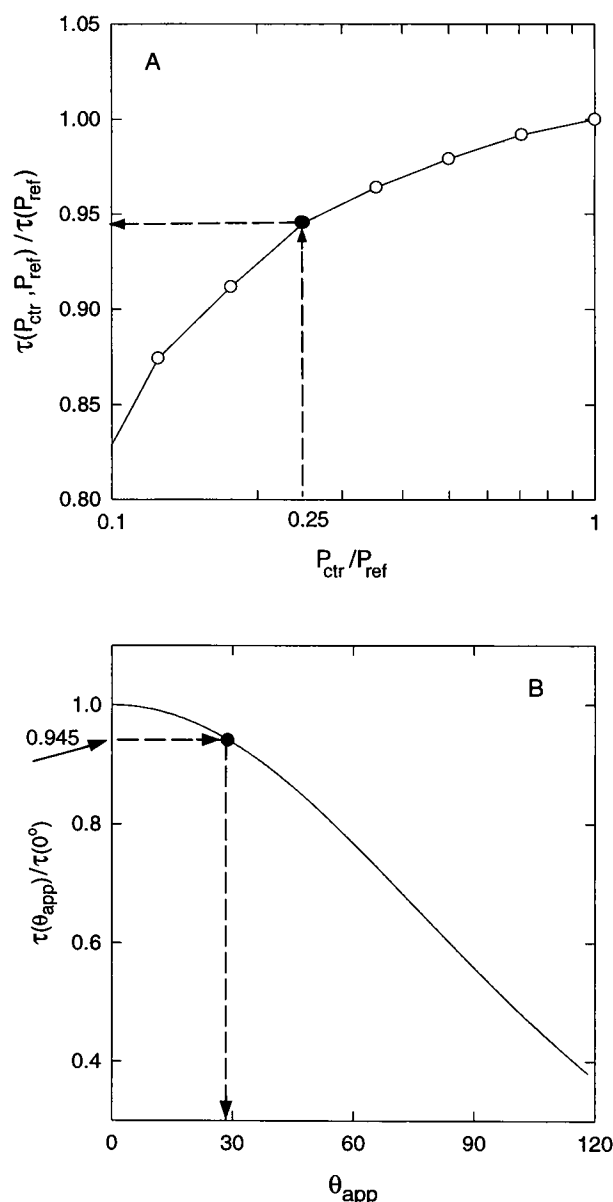

FIGURE 4   Example of the shift in the apparent bend angle (θ_{app}; derived from the τ-ratio) as a consequence of increased flexibility (angle dispersion) about a fixed angle, θ_o. In this example $\theta_o = 0°$, demonstrating the effect of pure added flexibility. (A) Plot of the computed τ-ratios for a 160-bp molecule possessing a 10-bp region of increased flexibility ($P_{ctr} < P_{ref}$) at the center of the molecule (see Methods). $P_{ref} = 700$ Å for the control helix and for the regions flanking the central 10 bp of the test molecule. The dashed lines with arrowheads indicate that for $P_{ctr}/P_{ref} = 0.25$, the computed τ-ratio is 0.946. (B) The computed τ-ratio in A (0.946) yields an apparent angle of ~27°.

bends (Zacharias and Hagerman, 1995a), this assumption is reasonable; however, for studies of more extended elements, such as the yeast tRNA^{Phe} core (Friederich et al., 1995), the self-cleaving RNA hammerhead (Amiri and Hagerman, 1994), or symmetrical internal loops (Zacharias and Hagerman, 1996), there is a residual uncertainty in the span (equivalent contour length) of the nonhelix element. To gauge the significance of this uncertainty, we have deter-
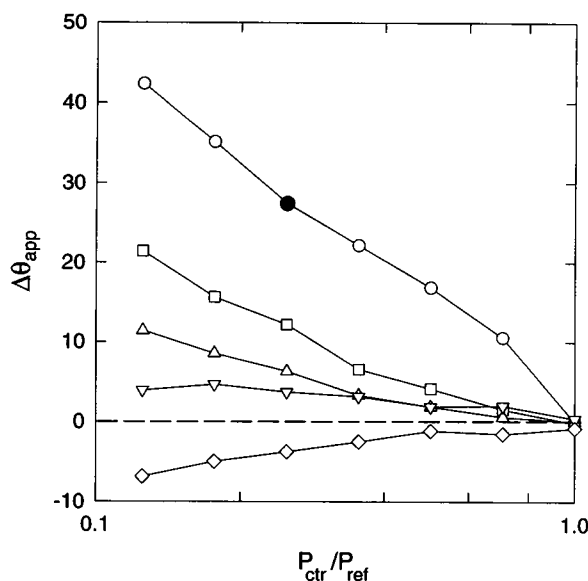
FIGURE 5 Plots of the difference ($\Delta\theta_{app}$) between θ_{app} and θ_o as a function of P_{ctr}/P_{ref} for the central, 10-bp region described in Fig. 4. Individual curves refer to fixed angles as follows: $\bigcirc$, 0°; $\square$, 30°; $\triangle$, 60°; ∇, 90°; $\Diamond$, 120°. The solid symbol refers to $\Delta\theta_{app}$ for the example presented in Fig. 4.

mined the relationship between the apparent angle and the true angle for various (introduced) length errors (Fig. 6).

First, for any given helix length and length error, the resulting error in the derived angle increases as the true angle decreases (Fig. 6). The origin of this behavior can be understood by noting the shape of the τ-ratio plots in Fig. 3. Specifically, very small changes in experimental τ-ratio for angles near zero leads to large changes in apparent angle, a consequence of the approximate cos θ behavior of the τ-ratio. Second, for any given angle and length error, the resulting error in the derived angle decreases as the overall helix length increases (Fig. 6, A–C). This latter effect reflects the fact that whereas the bend angle is essentially independent of the length chosen for the heteroduplex and duplex molecules (Fig. 3), the error in the apparent angle scales as the error in span length over the entire length of the heteroduplex. Thus, if the estimated span for a nonhelix element (true bend angle, 60°) is in error by the equivalent of 2 bp, the apparent angle would be in error by 13% for a 60-bp molecule, 6% for a 120-bp molecule, and 3% for a 180-bp molecule. In fact, the explicit examination of the length dependence of a derived bend angle can, in principle, be used as a means for refining the span length for the nonhelix element.

τ-ratio plots demonstrate maximum sensitivity when the bend element is located at the center of the helix

In the standard τ-ratio approach, a nonhelix element is placed at the center of a much longer helix to maximize the
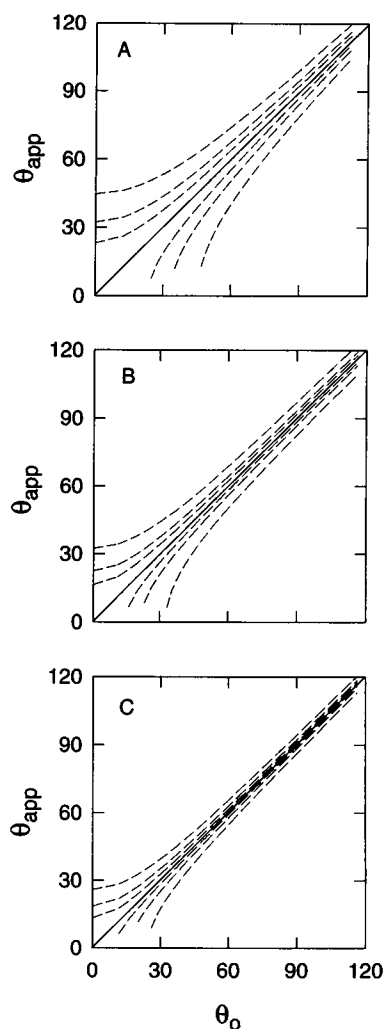

FIGURE 6 Effects of errors in the estimated length of a central, nonhelix element on apparent bend angle, θ_{app}, for specified values of the fixed angle, θ_o. The pairs of dashed lines represent errors of ± 1, ± 2, and ± 4 bp for chains of length (A) 60 bp; (B) 120 bp; and (C) 180 bp. If the molecule possessing the central bend is shorter than the control molecule, $\tau/\tau(0)$ will be further decreased, resulting in an apparent angle that is larger than the true angle (i.e., $\theta_{app} > \theta_o$). Errors in θ_{app} decrease as the lengths of both the straight and bent molecules are increased (A–C).

hydrodynamic consequences (i.e., minimize the τ-ratio) of any element-associated bend. The magnitude of this position effect can be appreciated by inspection of Fig. 7, in which sets of τ-ratio plots are displayed for bends placed at various positions along the helix contour. As the position of the bend is moved from 0.1 (fractional contour length) to 0.5 (center), the τ-ratio shift increases by roughly fourfold (a fourfold gain in sensitivity) over a broad range of angles (Fig. 7 B). Moreover, the shift in τ-ratio is relatively insensitive to length over the range examined (80–160 bp) (Fig. 7 C). These observations underscore one advantage (sensitivity) of centrally placed nonhelix elements. However, there is a second advantage of central placement, namely, that direct hydrodynamic contributions from the nonhelix element (e.g., short hairpins) are minimized
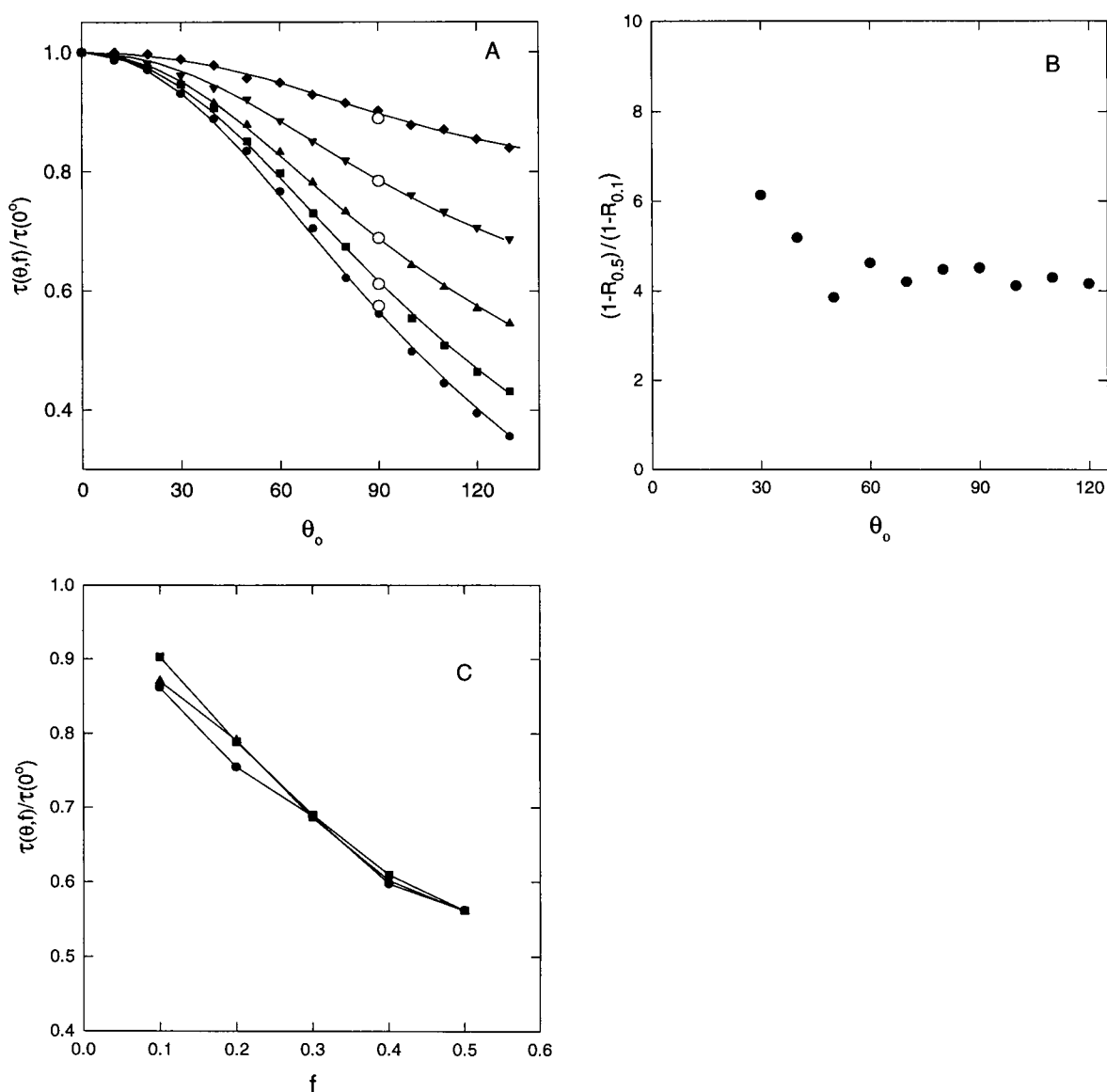
FIGURE 7 (A) Plots of the τ-ratio curves for fixed bends located at various positions along the helix contour for a 120-bp helix. Bends are located at fractional (f) contour positions of 0.1 ($\blacklozenge$), 0.2 ($\blacktriangledown$), 0.3 ($\blacktriangle$), 0.4 ($\blacksquare$), or 0.5 (center) ($\bullet$). Corresponding values for DNA helix parameters (rise/bp, 3.4 Å; hydrodynamic radius, 13 Å; persistence length, 500 Å) are also displayed ($\bigcirc$). (B) Plot of $(1 - R_{f = 0.5})/(1 - R_{f = 0.1})$ as a function of θ; $R = \tau(\theta)/\tau(0°)$. (C) Plots of the τ-ratio versus bend position for a 90° angle, and for three different helix lengths: 80 bp ($\bullet$), 120 bp ($\blacksquare$), and 160 bp ($\blacktriangle$).

when such elements are placed near the center of frictional resistance—an important advantage of hydrodynamic methods that exploit rotational diffusion as opposed to translational diffusion.

Two-bend phasing experiments present an approach for the direct evaluation of the intrinsic flexibility of individual bends

As indicated above, only in special circumstances (e.g., zero fixed bend) can information regarding bend flexibility be obtained from TEB measurements on individual bends. However, this limitation is lifted if one considers two adjacent, phased bends. For example, in the case of two fixed

bends (each of $\theta°$) in *cis*, the overall bend angle will approach 2θ, whereas for the same two angles positioned in *trans*, the arms will approach a parallel arrangement. Thus one would expect a strong phase dependence of the τ-ratio for two fixed bends, whereas two points of isotropic flexibility (each of $\langle\theta°\rangle_{rms}$) would yield an overall (apparent) bend angle of $\sim2^{1/2} \times \langle\theta°\rangle_{rms}$, with no phase dependence. One can therefore predict the expected τ-ratio behavior for a two-bend system from the single-bend results (apparent θ) and various models for bend dispersion. This approach is demonstrated in Fig. 8 for the case of an RNA helix with two 90° bends, and with variable degrees of additional lateral or torsional flexibility; essentially identical results are obtained by using DNA helix parameters (not shown).
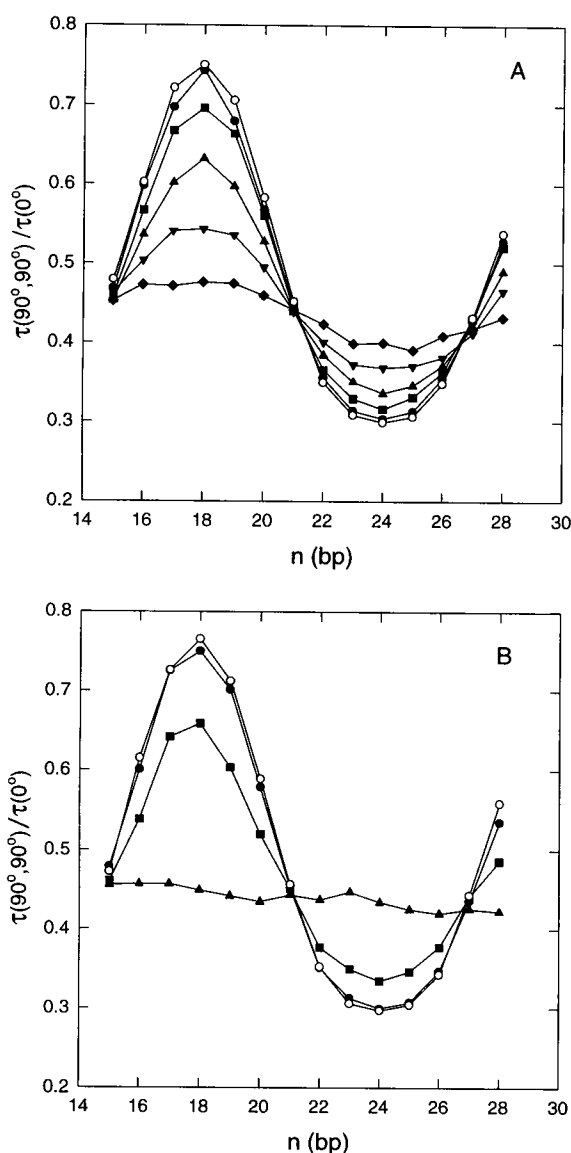
used to distinguish between added flexural and added torsional flexibility (Fig. 9). Not surprisingly, reduced torsional rigidity causes more rapid reduction in phasing amplitude with increasing bend separation. For this example, the torsional elastic constant has been reduced throughout the span separating the two bends—clearly an oversimplification. Moreover, the distinction will be enhanced for directional increases in bend dispersion (the current example represents isotropic dispersion).

The presence of an additional, short helix stem at the bend center introduces a minor, correctable effect on the apparent bend angle

For nonhelix elements that are created by the conjunction of three or more helices, examination of the interhelix angles involves the pairwise extension of the helix stems (e.g., Cooper and Hagerman, 1989; Shen and Hagerman, 1994; Amiri and Hagerman, 1994). In this situation, the nonextended helix is expected to contribute to the overall hydrodynamic drag experienced by the extended heteroduplex, resulting in an increase in the τ-ratio for any given bend angle relative to the τ-ratio for the same bend in the absence of the short (nonextended) helix. The magnitude of this effect will depend on 1) the relative lengths of the nonextended and extended helices, 2) the bend angle, and 3) the direction of the nonextended helix with respect to the direction of the bend. These factors are necessarily addressed by experiment; however, a rough estimate for the upper
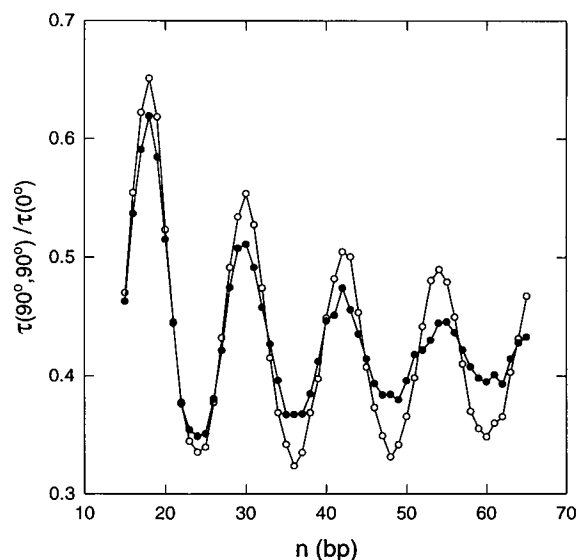
FIGURE 8   Plots of the τ-ratio, $\tau(90°, 90°)/\tau(0°)$, for molecules with two 90° bends separated by a helix segment of n bp. Bends (⇑) are positioned along the helix as follows: (70 bp) - ⇑ - (n bp) - ⇑ - (70 bp) for a total chain length of $(140 + n)$ bp. For the current example, the helix repeat has been set to 12 bp. (A) Fixed bends in the context of locally reduced persistence length: 10-bp regions with reduced persistence length (P_{ctr}) are centered on each bend (see Fig. 4), where $P_{ctr}/P_{ref} = 1$ (○), 0.5 (●), 0.25 (■), 0.125 (▲), 0.0625 (▼), and 0.031 (◆). The torsional elastic constant, C, has been set to 3.0×10^{-19} erg-cm (C_{ref}). (B) Fixed bends in the context of locally reduced torsional elastic constant: $C \approx \infty$ (○), 3.0 (●), 0.3 (■), 0.03 (▲) (units of 10^{-19} erg-cm). $P_{helix} = 700$ Å.

Although such an approach is not expected to completely define the nature of additional flexibility, it should provide an initial indication of the magnitude of such effects. In this regard, it is hoped that the inclusion of information from relative TEB decay amplitudes will augment the phasing studies (Zacharias and Hagerman, 1997).

Finally, for bend elements that possess additional flexibility, the two-bend phasing analysis can, in principle, be

FIGURE 9   Comparison of reduced P_{ctr} versus reduced C on the phase dependence of the τ-ratio over several helix turns for molecules with two 90° bends separated by n bp; helix lengths, bend locations, and helix parameters are as specified in Fig. 8. ○, $P_{ctr}/P_{ref} = 0.125$ for two 10-bp segments centered on bends; ●, $C_{ctr}/C_{ref} = 0.073$. Both modifications were chosen to yield reductions in the *trans* τ-ratios for $n = 18$ bp (*trans* orientation of bends) comparable to the values obtained in the absence of additional flexibility (Fig. 8).

bound for such contributions can be made by adding hydrodynamic beads along the angle bisector, in a direction opposite the subtended (interhelix) angle.

The results of a set of computations for nonextended helices with lengths that are 12.5% and 25% of the extended, single arm length are displayed in Fig. 10. For a bend at the center of a 160-bp helix, those extensions correspond to 10 bp and 20 bp, respectively. It is evident that even for the larger (25%) nonextended helix, the contribution to the τ-ratio is minor, with an increase of only 0.7% for the τ-ratio in the absence of a bend. This observation underscores one important attribute of rotational diffusion measurements alluded to above, namely that they are quite insensitive to the presence of an additional nucleic acid (or protein) surface near the center of diffusion. The contribution of the short stem increases with increasing bend angle, a consequence of the greater contribution of the short stem as it approaches "end-like" character. For example, a τ-ratio of 0.6, which corresponds to an angle of 83° in the absence of nonextended helix, yields upper bounds of 88° and 96° for nonextended helices of 12.5% and 25%, respectively. The "upper-bound" designation refers to the maximum hydrodynamic effect for short stems that are positioned along the angle bisector; different angular orientations would reduce the contribution of the nonextended helix. Interpolation (upper bound) functions corresponding to Eq. 2, given for the 12.5% and 25% extensions, are as follows:

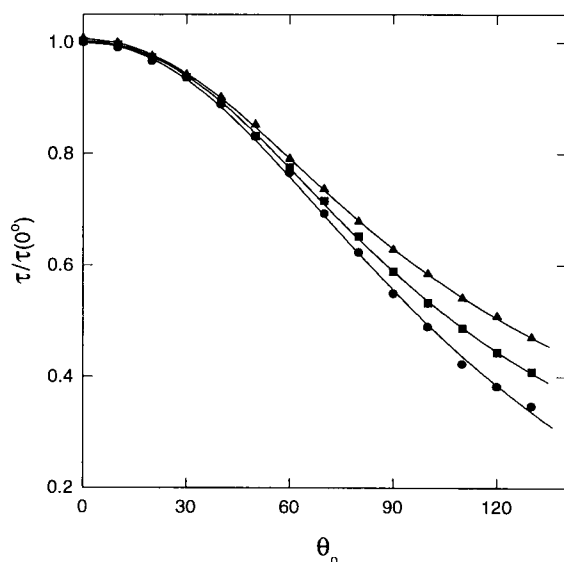$$\theta = a \times \cos^{-1}(R_{12.5} - k) + b \times [\sin^{-1}(1 - R_{12.5} + k)]^c \tag{3}$$

FIGURE 10 Dependence of the τ-ratio on the presence of an additional helix stem at the bend position. The additional helix stem is positioned on the angle bisector, extending away from the angle included between the main (80 bp) helix arms: ●, no additional helix; ■, 10-bp stem; ▲, 20-bp stem. Solid lines represent the corresponding interpolation formulae (Eqs. 2–4), fit to 130°.

with $a = 1.47$; $b = 0.0014$; $c = 2.81$; $k = 0.0019$, and

$$\theta = a \times \cos^{-1}(R_{25} - k) + b \times [\sin^{-1}(1 - R_{25} + k)]^c \tag{4}$$

with $a = 1.47$; $b = 0.0047$; $c = 2.59$; $k = 0.0069$. Equations 2–4 can be used to gauge the relationship between the τ-ratio and θ for various nonextended helix lengths. For example, the most acute interstem angle reported by Amiri and Hagerman (1994) for the self-cleaving hammerhead (111 ± 8°, between stems I and II) would be reduced by 3° (~3%) following correction for a 9–10 bp, nonextended helix III, a correction that is within the standard error of the reported angle. Finally, this analysis indicates that values for the contribution of nonextended helix stems might be estimated by varying the lengths of either the extended arms or the nonextended helix.

DISCUSSION

The current analysis has demonstrated that the τ-ratio approach, which restricts its focus to the terminal portion of the birefringence decay profile, is well suited to providing quantitative information about bends or points of increased flexibility in otherwise duplex (helical) nucleic acids. In particular, when the birefringence decay profile of a double-stranded molecule possessing a centrally located, nonhelix element is compared with its full-duplex counterpart, the resulting τ-ratio is quite insensitive to uncertainties in the intrinsic flexibility and structural/hydrodynamic properties of the native helix. This insensitivity simply reflects the fact that for heteroduplex and duplex molecules of identical sequence (apart from the central element), the hydrodynamic consequences of sequence-dependent variations in flexibility, rise, etc., will largely cancel in the τ-ratio. This principle can be exploited further in those instances where there exists significant uncertainty in the span of the element being studied, because the consequent uncertainty in the derived angle decreases as the length of the flanking helix increases. As anticipated, the current results also demonstrate that the greatest experimental sensitivity obtains for elements that are flanked by helices of equal length, in agreement with earlier observations for rigid rods (Iniesta et al., 1988).

The issue of excess flexibility and/or angular isomerism is generally difficult to address with single TEB measurements, because the τ-ratio reflects contributions from any additional angular dispersion about a bend of minimum energy. In particular, depending on the dimensionality of the dispersion, the mean angle in solution (reflecting minimum free energy) may be different from the angle of minimum potential energy, as might be observed in a crystal structure. Thus this shift does not represent a bias of the TEB/τ-ratio method itself. However, because the ensemble average is a diffusion average, the method itself will introduce a slight bias toward larger bend angles (smaller subtended angles), in the same direction as the bias introduced

by methods involving resonance energy transfer (weighted as R^{-6}), although less severe (i.e., weighted as $1/\tau$, $\sim R^{-n}$, $n < 3$).

For the special case in which the heteroduplex and full-duplex species have identical decay profiles (i.e., a τ-ratio of unity and identical fast decay components), as observed for the transactivation response element (TAR)-Tat peptide complex (Zacharias and Hagerman, 1995b), one can conclude that the nonhelix element is neither significantly bent, nor more flexible than the surrounding helix, because any angular dispersion would reduce the τ-ratio. A somewhat different situation exists in the instance of a τ-ratio of unity, but where the heteroduplex species manifests a substantially larger fast component than the duplex. In the absence of uncertainty in the span of the element, the τ-ratio suggests that the most extended species within the population of heteroduplex molecules are essentially linear, but that significant populations of less extended conformers also exist, and that the conformers are likely to be in slow exchange on the TEB time scale (see Shen and Hagerman, 1994). Clearly, more work is needed in this area.

Finally, the current results have outlined an approach to the study of bend dispersion/isomerism using a two-bend heteroduplex in which the helical phasing of the two bends is varied. Specification of the apparent angle from a single-bend τ-ratio yields a two-bend, phased τ-ratio plot with added lateral and torsional dispersion as the only adjustable parameters. Thus, in the absence of excess dispersion, one should be able to place a lower bound on the torsional elastic constant for the RNA segment separating the two bends.

CONCLUSIONS

The current work has provided a systematic examination of the utility of the τ-ratio approach for quantifying interhelix angles and for providing evidence of increased flexibility of simple, nonhelix elements in DNA and RNA. Although the τ-ratio approach is a static representation of the diffusion process, it has been shown to be an accurate representation thereof, and is far easier to implement than various dynamic methods. However, the current method, by its nature, is not able to interpret the faster component of the decay process; such an interpretation requires dynamic methods. One example of this latter approach is the subject of the accompanying paper (Zacharias and Hagerman, 1997). Taken together with the TEB method, the static and dynamic approaches represent a powerful set of tools for the study of global tertiary structure in nucleic acids.

REFERENCES

Allison, S. A., and P. Nambi. 1992. Electric dichroism and birefringence decay of short DNA restriction fragments studied by Brownian dynamics simulation. *Macromolecules.* 25:759–768.

Amiri, K. M. A., and P. J. Hagerman. 1994. Global structure of a self-cleaving hammerhead RNA. *Biochemistry.* 33:13172–13177.

Charney, E. 1988. Electric linear dichroism and birefringence of biological polyelectrolytes. *Q. Rev. Biophys.* 21:1–60.

Cooper, J., and P. J. Hagerman. 1989. Geometry of a branched DNA structure in solution. *Proc. Natl. Acad. Sci. USA.* 86:7336–7340.

Diekmann, S., W. Hillen, M. Jung, R. D. Wells, and D. Porschke. 1982. Electric properties and structure of DNA restriction fragments from measurements of the electric dichroism. *Biophys. Chem.* 15:157–167.

Fredericq, E., and C. Houssier. 1973. Electric Dichroism and Electric Birefringence. Clarendon, Oxford, England.

Friederich, M., F.-U. Gast, E. Vacano, and P. J. Hagerman. 1995. Determination of the angle between the anticodon and aminoacyl acceptor stems of yeast phenylalanyl tRNA in solution. *Proc. Natl. Acad. Sci. USA.* 92:4803–4807.

Garcia de la Torre, J., and V. A. Bloomfield. 1980. Conformation of myosin in solution as estimated from hydrodynamic properties. *Biochemistry.* 19:5118–5123.

Garcia de la Torre, J., and V. A. Bloomfield. 1981. Hydrodynamic properties of complex, rigid, biological macromolecules: theory and applications. *Q. Rev. Biophys* 14:81–139.

Garcia de la Torre, J., P. Mellado, and V. Rodes. 1985. Diffusion coefficients of segmentally flexible macromolecules with two spherical subunits. *Biopolymers.* 24:2145–2164.

Garcia Molina, J. J., M. C. Lopez Martinez, and J. Garcia de la Torre. 1990. Computer simulation of hydrodynamic properties of semiflexible macromolecules: randomly broken chains, wormlike chains, and analysis of properties of DNA. *Biopolymers.* 29:883–900.

Hagerman, P. J. 1984. Evidence for the existence of stable curvature of DNA in solution. *Proc. Natl. Acad. Sci. USA.* 81:4632–4636.

Hagerman, P. J. 1988. Flexibility of DNA. *Annu. Rev. Biophys. Biophys. Chem.* 17:265–286.

Hagerman, P. J. 1996. "Sometimes a great motion": the application of transient electric birefringence to the study of macromolecular structure. *Curr. Opin. Struct. Biol.* 6:643–649.

Hagerman, P. J. 1997. Flexibility of RNA. *Annu. Rev. Biophys. Biomol. Struct.* (in press).

Hagerman, P. J., and V. A. Ramadevi. 1990. Application of the method of phage T4 DNA ligase-catalyzed ring-closure to the study of DNA structure. I. Computational analysis. *J. Mol. Biol.* 212:351–362.

Hagerman, P. J., and B. Zimm. 1981. Monte Carlo approach to the analysis of the rotational diffusion of wormlike chains. *Biopolymers.* 20: 1481–1502.

Harvey, S. C., and H. Cheung. 1980. Transport properties of particles with segmental flexibility. II. Decay of fluorescence polarization anisotropy from hinged macromolecules. *Biopolymers.* 19:913–930.

Harvey, S. C., and H. C. Cheung. 1982. Myosin flexibility. *In* Cell and Muscle Motility, Vol. 2. R. M. Dowben and J. W. Shay, editors. Plenum, New York. 279–302.

Harvey, S. C., P. Mellado, and J. Garcia de la Torre. 1983. Hydrodynamic resistance and diffusion coefficients of segmentally flexible macromolecules with two subunits. *J. Chem. Phys.* 78:2081–2090.

Highsmith, S., K. M. Kretzschmar, C. O'Konski, and F. Morales. 1977. Flexibility of myosin rod, light meromyosin and myosin subfragment-2 in solution. *Proc. Natl. Acad. Sci. USA.* 74:4986–4990.

Highsmith, S., C. C. Wang, K. Zero, R. Pecora, and O. Jardetzky. 1982. Bending motions and internal motions in myosin rod. *Biochemistry.* 21:1192–1197.

Iniesta, A., F. G. Diaz, and J. Garcia de la Torre. 1988. Transport properties of rigid bent-rod macromolecules and of semiflexible broken rods in the rigid-body treatment. Analysis of the flexibility of myosin rod. *Biophys. J.* 54:269–275.

Kebbekus, P., D. E. Draper, and P. Hagerman. 1995. Persistence length of RNA. *Biochemistry.* 34:4354–4357.

Kramers, H. A. 1946. The behavior of macromolecules in inhomogeneous flow. *J. Chem. Phys.* 14:415–424.

Leehey, M. A., C. A. Squassoni, M. W. Friederich, J. B. Mills, and P. J. Hagerman. 1995. A non-canonical tertiary conformation of a human mitochondrial transfer RNA. *Biochemistry.* 34:16236–16239.

Levene, S. D., H.-M. Wu, and D. M. Crothers. 1986. Bending and flexibility of kinetoplast DNA. *Biochemistry.* 25:3988–3995.

Mellado, P., and J. Garcia de la Torre. 1982. Steady state and transient electric birefringence of solutions of bent-rod macromolecules. *Biopolymers.* 21:1857–1871.

Mellado, P., A. Iniesta, F. G. Diaz, and J. Garcia de la Torre. 1988. Diffusion coefficients of segmentally flexible macromolecules with two subunits: a study of broken rods. *Biopolymers.* 27:1771–1786.

O'Konski, D. T., editor. 1976. Molecular Electro-Optics. Marcel Dekker, New York.

Porschke, D., E. R. Schmidt, T. Hankeln, G. Nolte, and J. Antosiewicz. 1993. Structure and dynamics of curved DNA fragments in solution: evidence for slow modes of configurational transitions. *Biophys. Chem.* 47:179–191.

Roitman, D. B. 1984. An elastic hinge model for dynamics of stiff chains. III. Viscoelastic and Kerr-effect behavior of bent molecules. *J. Chem. Phys.* 81:6356–6360.

Roitman, D. B., and B. Zimm. 1984a. An elastic hinge model for dynamics of stiff chains. I. Viscoelastic properties. *J. Chem. Phys.* 81:6340–6347.

Roitman, D. B., and B. Zimm. 1984b. An elastic hinge model for dynamics of stiff chains. II. Transient electro-optical properties. *J. Chem. Phys.* 81:6348–6354.

Rotne, J., and J. Prager. 1969. Variational treatment of hydrodynamic interactions in polymers. *J. Chem. Phys.* 50:4831–4837.

Schellman, J. A. 1974. Flexibility of DNA. *Biopolymers.* 13:217–226.

Shen, Z., and P. J. Hagerman. 1994. Geometry of the central branch of the 5S ribosomal RNA of *Sulfolobus acidocaldarius*. *J. Mol. Biol.* 241: 415–430.

Stellwagen, N. 1991. Transient electric birefringence of two small DNA restriction fragments of the same molecular weight. *Biopolymers.* 31: 1651–1667.

Taylor, W. H., and Hagerman, P. J. 1990. Application of the method of T4 DNA ligase-catalyzed ring-closure to the study of DNA structure. II. NaCl-dependence of DNA flexibility and helical repeat. *J. Mol. Biol.* 212:363–376.

Wegener, W. A. 1982a. Bead models of segmentally flexible macromolecules. *J. Chem. Phys.* 76:6425–6430.

Wegener, W. A. 1982b. A swivel-jointed formalism for segmentally flexible macromolecules and its application to the rotational behavior of myosin. *Biopolymers.* 21:1049–1080.

Wegener, W. A. 1986. Transient electric birefringence of dilute rigid-body suspensions at low field strength. *J. Chem. Phys.* 84:5989–6004.

Wegener, W. A., R. M. Dowben, and V. J. Koester. 1979. Time-dependent birefringence, linear dichroism, and optical rotation resulting from rigid-body rotational diffusion. *J. Chem. Phys.* 70:622–632.

Wegener, W. A., R. M. Dowben, and V. J. Koester. 1980. Diffusion coefficients for segmentally flexible macromolecules: general formalism and application to rotational behavior of a body with two segments. *J. Chem. Phys.* 73:4086–4097.

Zacharias, M., and P. J. Hagerman. 1995a. Bulge-induced bends in RNA: quantification by transient electric birefringence. *J. Mol. Biol.* 247: 486–500.

Zacharias, M., and P. J. Hagerman. 1995b. The bend in RNA created by the trans-activation response element bulge of human immunodeficiency virus is straightened by arginine and by Tat-derived peptide. *Proc. Natl. Acad. Sci. USA.* 92:6052–6056.

Zacharias, M., and P. J. Hagerman. 1996. The influence of symmetric internal loops on the flexibility of RNA. *J. Mol. Biol.* 257:276–289.

Zacharias, M., and P. J. Hagerman. 1997. Influence of static and dynamic bends on the conformation of RNA: Brownian dynamics simulations. *Biophys. J.* 73:318–332.

Zimm, B. H. 1980. Chain molecule hydrodynamics by the Monte Carlo method and the validity of the Kirkwood-Riseman approximation. *Macromolecules.* 13:592–602.